Mechanical properties of highly oriented FeSe0.5Te0.5 superconductor

Jorge Luiz Pimentel Júnior, Paulo Pureur, Cristiano Santos Lopes, Francisco Carlos Serbena, Carlos Eugênio Foerster et al.

Citation: J. Appl. Phys. **111**, 033908 (2012); doi: 10.1063/1.3677948
View online: http://dx.doi.org/10.1063/1.3677948
View Table of Contents: http://jap.aip.org/resource/1/JAPIAU/v111/i3
Published by the American Institute of Physics.

Mechanical properties of highly oriented $FeSe_{0.5}Te_{0.5}$ superconductor

Jorge Luiz Pimentel Júnior,[1] Paulo Pureur,[1] Cristiano Santos Lopes,[2] Francisco Carlos Serbena,[2] Carlos Eugênio Foerster,[2] Simone Aparecida da Silva,[2] Alcione Roberto Jurelo,[2,a)] and Adilson Luiz Chinelatto[3]

[1]*Instituto de Física, Universidade Federal do Rio Grande do Sul, Caixa Postal 15.051, 91.501-970, Porto Alegre, Rio Grande do Sul, Brazil*

[2]*Departamento de Física, Universidade Estadual de Ponta Grossa, av. Gen. Carlos Cavalcanti 4748, 84.030-000, Ponta Grossa, Paraná, Brazil*

[3]*Departamento de Engenharia de Materiais, Universidade Estadual de Ponta Grossa, av. Gen. Carlos Cavalcanti 4748, 84030-000, Ponta Grossa, Paraná, Brazil*

(Received 13 October 2011; accepted 17 December 2011; published online 6 February 2012)

We have synthesized highly oriented samples of the superconducting compound $FeSe_{0.5}Te_{0.5}$ and investigated its mechanical properties. These samples were characterized by scanning electron microscopy (SEM) with energy-dispersive analysis, x-ray diffraction, and electrical resistivity. The measured critical temperature is $T_C \sim 14.5$ K. Hardness and elastic modulus on the *ab*- and *a(b)c*-plane were obtained by instrumented indentation. The samples' morphology consists of plate-like crystals with a lamellar structure. Two phases were observed with a typically eutectic microstructure composed by white and gray lamellas when observed with SEM using backscattered electrons. The white phase is richer in Te and poorer in Se than the gray phase. No significant differences in hardness and elastic modulus were observed between *ab*- and *a(b)c*-planes. Hardness profiles indicated values in the range 0.6–0.8 GPa at deep tip penetration depths, while the elastic modulus showed values in between 20–25 GPa. Cracking was occasionally observed in the *ab*-plane and at low loads. © *2012 American Institute of Physics*. [doi:10.1063/1.3677948]

I. INTRODUCTION

Recently, superconductivity was observed in FeSe compounds with a critical temperature $T_C = 8$ K.[1] The FeSe phase diagram shows two major phases, α and β.[2,3] The $\beta-$phase is stoichiometric, nonmagnetic, and nonsuperconducting. Meanwhile, the $\alpha-$phase is magnetic and superconducting when the Se content is slighly substoichiometric. The presence and concentration of each phase depend on the elemental composition, synthesis process, and conditions of temperature, or pressure. The phase $\alpha-FeSe_{1-x}$ is the simplest-structured among the iron-based superconductors. Its anti-PbO type structure is composed of a stack of edge sharing $FeSe_4$ tetragonal layer by layer belonging to the $P4/nmm$ space group.[4,5]

The compound FeTe is structurally analogous to the superconducting $\alpha-$FeSe. However, the physical properties of these compounds are distinct and depend on the excess of Fe at the interlayer site.[6] Although FeTe is non-superconducting, the critical temperature of FeSe is increased by partially substituting Se for Te. The maximum value $T_C = 15$ K is attained for the composition $FeSe_{0.5}Te_{0.5}$.[6] This critical temperature increases up to 26 K when an external pressure of approximately 2 GPa is applied.[7] Although FeSe and FeTe are isostructural at room temperature, they show different behavior upon cooling. FeTe undergoes simultaneous structural (tetragonal to monoclinic) and antiferromagnetic transitions at $T_N \sim 70$ K.[8,9] FeSe shows a structural transition from the tetragonal symmetry to an orthorhombic phase in the interval 70–90 K. Contrasting with the $\alpha-$FeSe phase, $\alpha-$FeTe is structurally much more stable, and can be easily obtained by using a conventional solid-state reaction method, even at synthesis temperatures as high as 1200 K.[10,11]

Among the Fe-based superconductors, the FeSe(Te) compound is expected to play an important role for understanding the real mechanism promoting superconductivity in the systems. However, detailed investigations of the intrinsic nature of superconductivity require high quality single crystals samples. This is also the case for the study of mechanical properties in this compound, such as hardness, elastic modulus, and fracture toughness. In polycrystalline samples, the existence of secondary phases and grain boundaries makes difficult the characterization of the compound's intrinsic mechanical properties.

In this work, we measured the hardness and the elastic modulus of highly oriented $FeSe_{0.5}Te_{0.5}$ samples using instrumented indentation. These samples were characterized by scanning electron microscopy (SEM) with energy-dispersive analysis (EDS), x-ray diffraction (XRD), and electrical resistivity. The measured critical temperature is $T_C \sim 14.5$ K. Two phases with a typically eutectic microstructure were observed to occur, one being richer in Te while the other is richer in Se. The measured hardness and elastic modulus are approximately the same for two phases. The values obtained for these properties are influenced by the stacking of planes parallel to the *ab*-atomic planes characteristic of the studied compound.

II. EXPERIMENTAL DETAILS

Highly oriented superconductors of $FeSe_{0.5}Te_{0.5}$ have been produced using a self-flux method. Appropriate

a)Author to whom correspondence should be addressed. Electronic mail: arjurelo@uepg.br

amounts of Fe (99.99%) pieces, Te (99.9%) shots, and Se (99.9%) shots were mixed, grounded, and pressed into a pellet, that was loaded into a silica ampoule, evacuated and sealed. The piece was melted at 1000 °C for 15 min, then cooled slowly at a temperature rate of approximately 5 °C/h down to 400 °C, followed by furnace cooling to room temperature. Several highly textured samples could be cut out from the melted monolith. Some of them were selected for present investigation. X-ray diffraction of the chosen samples were performed using a Siemens diffractometer with $CuK\alpha$ radiation and a scanning rate of 0.02° per second and a $\theta - 2\theta$ scan from 10° to 70°. The resistance measurements with current in the *ab*-plane were performed with a Quantum Design Physical Properties Measurement System (PPMS), using the standard four-probe method. Elastic modulus profiles were determined by instrumented indentation following the Oliver and Pharr method[12] and using a Nanoindenter XP™. The indentations were performed using a diamond Berkovich indenter with applied loads ranging from 10 to 50 mN parallel and perpendicular to the *c*-axis. Within this load range, the mechanical properties of regions near the surface and inside the single crystals could be measured. Due to the difficulty in obtaining perfect and planar large regions on the *ab*-plane due to the lamellar fracture, regions for each indentation were chosen individually using an optical microscope coupled with the nanoindenter prior to the indentations. For the measures in the *a(b)*c-plane, samples were mounted in a low-cure temperature resin and polished. Finishing was achieved with 1 μm diamond paste. The microstructures were observed with optical and scanning electron microscopy equipped with energy-dispersive analysis. The contents of Fe, Se, and Te were determined across the cleaved section parallel or perpendicular to the square planar layers formed by iron-pnitide atomic planes.

III. RESULTS AND DISCUSSION

Figure 1(a) shows the SEM micrograph of one typical highly oriented $FeSe_{0.5}Te_{0.5}$ sample. Shining plate-like crystals were observed with dimensions ranging between 2–3 mm in the planar orientation and 50 μm thick. The shape of the sample, as well as the fact that the crystals can easily be cleaved, reveal the highly layered structure characteristics of this material. Figure 1(b) shows in higher magnification the lamellar structure of the sample.

Figure 2 show the SEM micrograph perpendicular to the *c*-axis of another $FeSe_{0.5}Te_{0.5}$ sample. In Fig. 2(a), we can observe two phases, labeled white and gray. In Figs. 2(b) and 2(c) are shown amplifications of panel(a), where besides the white and gray phases, a typically eutectic microstructure, composed by white and gray lamellas, can be observed. The compositions of the white and gray phases measured by EDS are shown in Table I. One observes that the white phase is richer in Te and poorer in Se when compared with the gray phase.

Typical XRD data are shown in Fig. 3, where we can observe only the $(00l)$ peaks, illustrating that the $FeSe_{0.5}Te_{0.5}$ sample is exclusively oriented along the $c-$axis. The crystal symmetry is described by a tetragonal PbO structure with the $P4/nmm$ space group, consistent with previously reported results.[4,5] As observed in Fig. 1(b), the sample consists of several stacked lamellas. From the XRD analysis, one obtains that the larger surface of each lamella is perpendicular to the *c*-axis. However, no planar ordering occurs, so that each lamella can have a different orientation with respect to the *a* and *b* directions. Ge *et al*. observed a similar structure as ours using SEM in $Fe_{1.03}Te_{0.55}Se_{0.45}$ samples.[3] From Laue diffraction patterns and XRD diffraction, they concluded that their material was not a single crystal, but a highly oriented sample.[3]

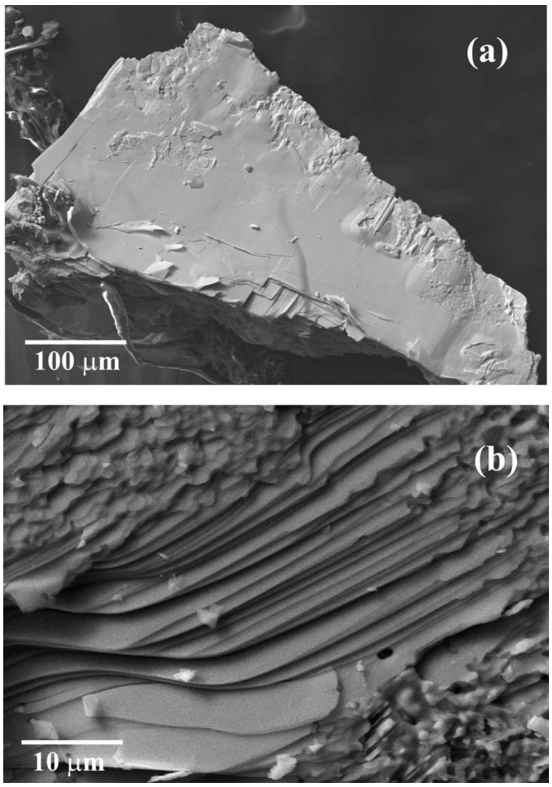

FIG. 1. (a) Scanning electron microscopy image for a highly oriented $FeSe_{0.5}Te_{0.5}$ sample. Panel (b) shows a higher magnification of the lamellar structure of the sample.

Figure 4 shows the temperature dependence of the in-plane resistivity in a broad temperature window for a representative $FeSe_{0.5}Te_{0.5}$ melt-textured sample. The applied current was $I = 1$ mA and the room-temperature resistivity was $\rho(300\ \mathrm{K}) = 2.7\ \mathrm{m}\Omega\,\mathrm{cm}$. The resistivity increases slightly upon decreasing temperatures down to 180 K approximately, goes through a flat and broad maximum around 150 K, then decreases strongly when the temperature is further lowered. Superconductivity sets at $T_C \cong 14.5$ K. The inset shows the resistivity in the temperature interval between 10 and 20 K. The transition width, ΔT, defined according to the criteria 5–95 % of the resistive transition, is approximately 0.6 K. This result indicates that our samples have good crystalline quality.

The origin of the semiconductor-like behavior observed in the high temperature range is unknown at this moment. Recent resistivity measurements by Liu *et al*. in $Fe_{1.12}Se_{0.33}Te_{0.72}$ (with a large amount of excess Fe) show semiconductor-like behavior down to T_C, while $Fe_{1.04}Se_{0.28}Te_{0.72}$ (with relative smaller Fe content) a metallic behavior is observed in the whole temperature range from 300 K

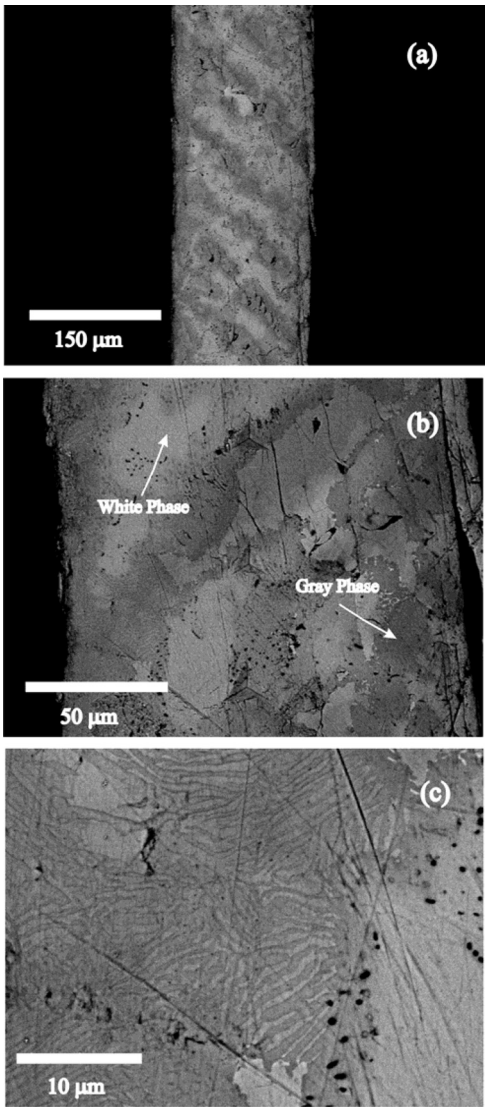

FIG. 2. SEM image of a highly oriented $FeSe_{0.5}Te_{0.5}$ sample perpendicular to the *c*-axis at different magnifications.

down to T_C.[13] According to the authors, the amount of interstitial Fe existing between the FeSe(Te) layers is the most important factor to produce this contrasting resistivity behavior.

Figures 5 show the deformation produced by Berkovich indentations at different loads on the *ab*-plane. At loads around 10 mN, radial cracks emanating from the corners of the indentation are occasionally observed. Also observed is that the material piles-up around the indentation and lateral cracks are nucleated at higher loads, as may be seen in Fig. 5(b). When these lateral cracks are nucleated, the radial cracks are suppressed. Increasing the load to 50 mN,

TABLE I. Composition of a nominally $FeSe_{0.5}Te_{0.5}$ sample as obtained from EDS analysis.

Composition	Fe	Se	Te
Initial	1.00	0.50	0.50
White phase	1.02	0.33	0.65
Gray phase	0.99	0.67	0.34

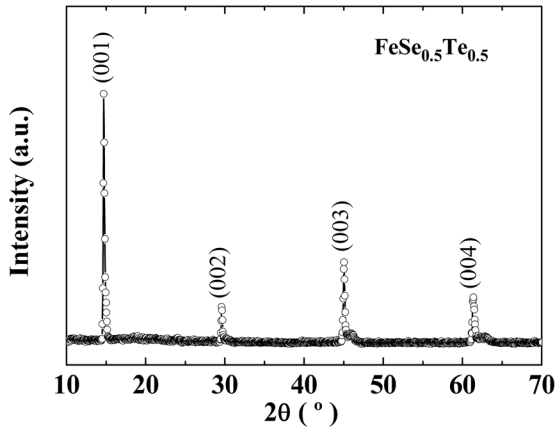

FIG. 3. X-ray diffraction pattern of $FeSe_{0.5}Te_{0.5}$.

cracking is more severe. Several cracks inside the impression are observed with no extension of radial cracks to longer distances from the impression limits. The morphology of the cracks suggests that they run parallel to the surface. At 100 mN, cracking is even more severe, with material detachment at the corners of the impression. A region with no lateral cracks is observed at the center of the indentation in Fig. 5(b). Its size is that of the order of the impression at 10 mN. This observation suggests that the load threshold for nucleation of these lateral cracks is below 10 mN.

Figure 6 show Berkovich indentations at different loads on the *a(b)c*-plane. At 10 mN, no cracks are visible. It appears from the image that the material sinks-in slightly, contrary to the observation of pile-up in the *ab*-plane. Increasing the load promotes the appearance of several cracks. Further increase in the load to 100 mN produces larger cracks inside and around the impression. These cracks run preferentially along the same direction, indicating that they are highly oriented. For this reason, we assume that the cracks are or between the *ab*-planes or between the individual lamellar single crystals.

Based on the previous observations in Figs. 5 and 6, we proposed in Fig. 7 a schematic representation of the cracking mechanism for an indentation in the *ab*-plane. As the

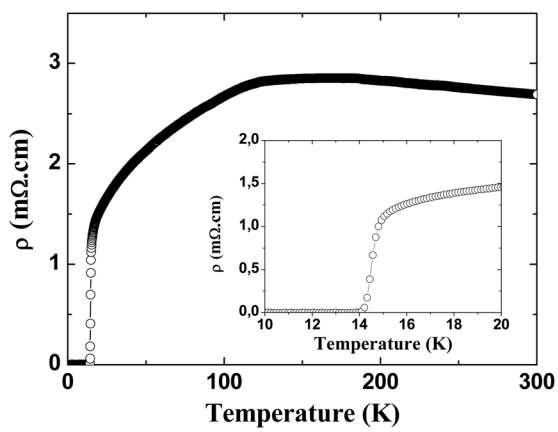

FIG. 4. Temperature dependence of the in-plane resistivity for $FeSe_{0.5}Te_{0.5}$. The inset presents results in the temperature range between 10 and 20 K. The critical temperature estimated at the half-width of the resistive transition is $T_C \cong 14.5$ K.

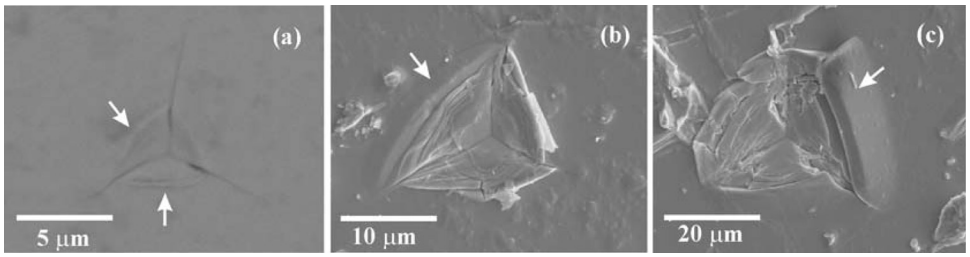

FIG. 5. SEM micrographs of Berkovich indentations on the *ab*-plane of $FeSe_{0.5}Te_{0.5}$ at (a) 10 mN, (b) 50 mN, and (c) 100 mN.

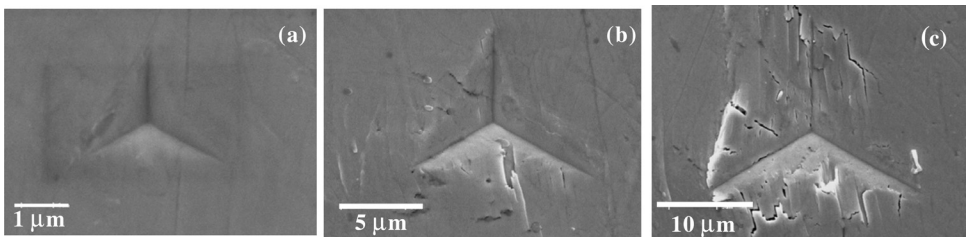

FIG. 6. SEM micrographs of Berkovich indentations at room temperature for *a(b)c*-plane of (a) 10 mN, (b) 50 mN, and (c) 100 mN for $FeSe_{0.5}Te_{0.5}$.

indenter penetrates in the sample, cracks parallel to the surface are nucleated at the edges of the indenter as indicated by arrows in Figs. 5. This mechanism is consisted with the crack pattern assumed as perpendicular to the *c*-axis observed in Fig. 5(c).

Figure 8 show typical loading-unloading curves for indentations in the *ab* and *a(b)c*-planes for a load of 50 mN. Several tip incursions are observed in the loading portion. This load corresponds to Figs. 5(b) and 6(b) where several cracks are observed around the impression. The tip incursions in the *ab*-plane can be related to the nucleation and propagation of lateral cracks where the tip loses support when the material underneath is displaced. In the *a(b)c*-plane, more tip incursions are observed and they are more pronounced. This might be related with the separation of the *ab*-planes shown in Fig. 1(b). These observations reflect the lamellar microstructure of this material.

Figure 9(a) and 9(b) show the hardness variation as a function of the contact depth for the *ab*- and *a(b)c*-planes. We observed individual indentations in the SEM using backscattered imaging to locate if they were in white or gray regions. When comparing the individual indentations with their respective hardness, we did not observe any difference between the white and gray regions. In Figs. 9(a) and 9(b) we identified using different symbols the phases where the indentations were located. Near the surface, the hardness is around 2.2 GPa for the *ab*-plane and 1.7 GPa for the *a(b)c*-plane. Increasing the load results in lower hardness for both planes: 0.8 and 0.6 GPa for the *ab*- and *a(b)c*-planes, respectively. These hardness are lower than that measured in polycrystalline $FeSe_x$ superconductor samples with different contents of the α-$FeSe_{1-x}$, β-$FeSe_{1-x}$, and Fe_7Se_8 phases. In this case, the observed hardness is 1.3 ± 0.2 GPa.[14,15]

Figure 10(a) and 10(b) show the elastic modulus versus the contact depth. We identified using different symbols the phases where the indentations were located. The elastic

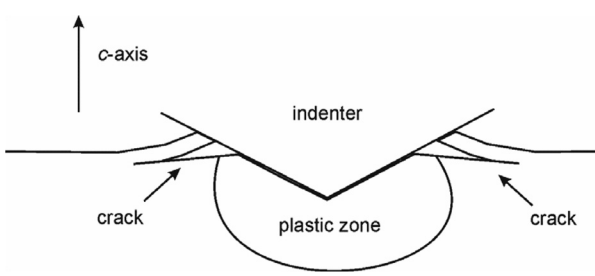

FIG. 7. Schematic representation of the cracking mechanism for indentations in the *ab*-plane of $FeSe_{0.5}Te_{0.5}$.

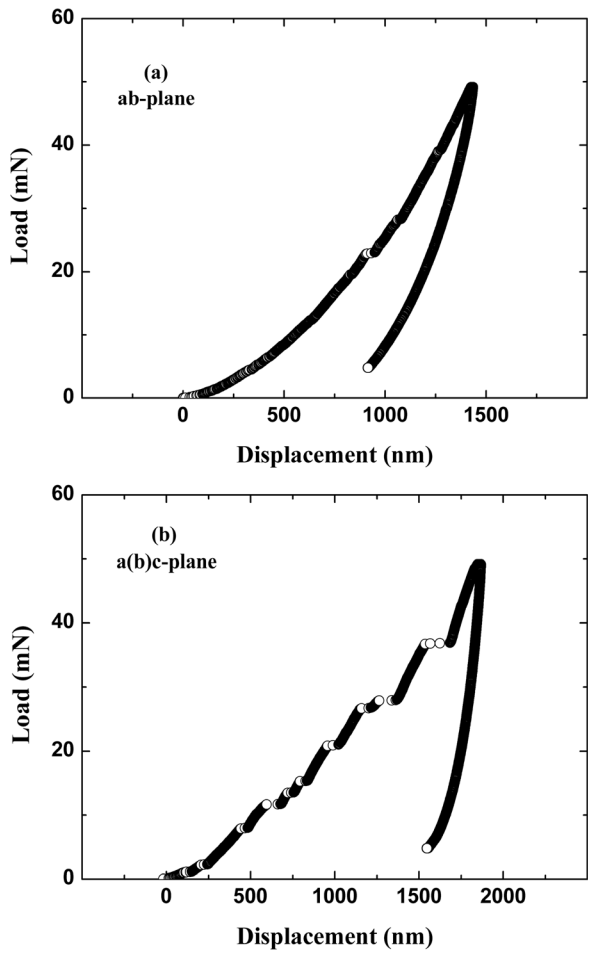

FIG. 8. Typical load-unloading curves for $FeSe_{0.5}Te_{0.5}$: (a) *ab*-plane and (b) *a(b)c*-plane.

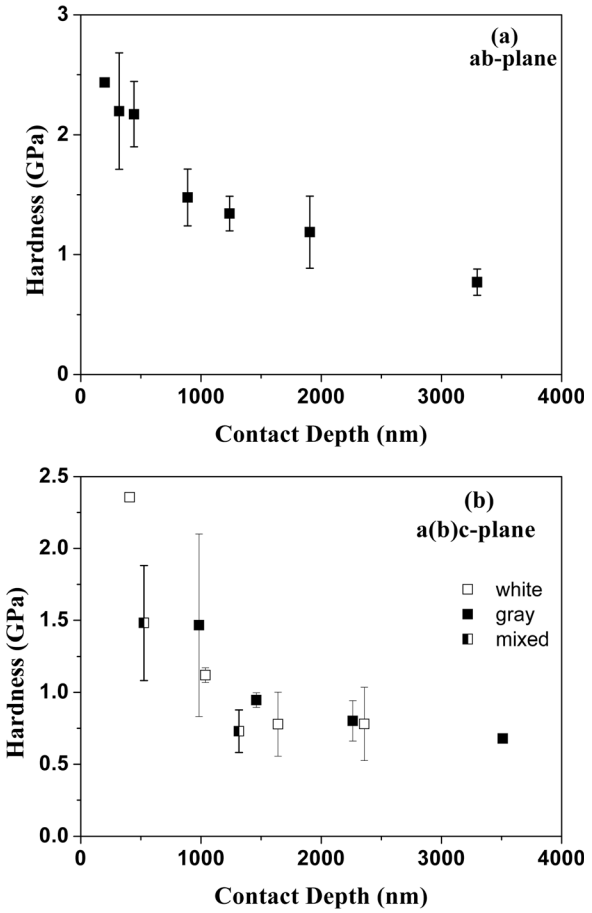

FIG. 9. Profiles of hardness as a function of contact depth for $FeSe_{0.5}Te_{0.5}$ in the (a) *ab*-plane and (b) *a(b)c*-plane. Indentations in gray, white, and mixed phases are represented by the symbols ■, □, and □, respectively.

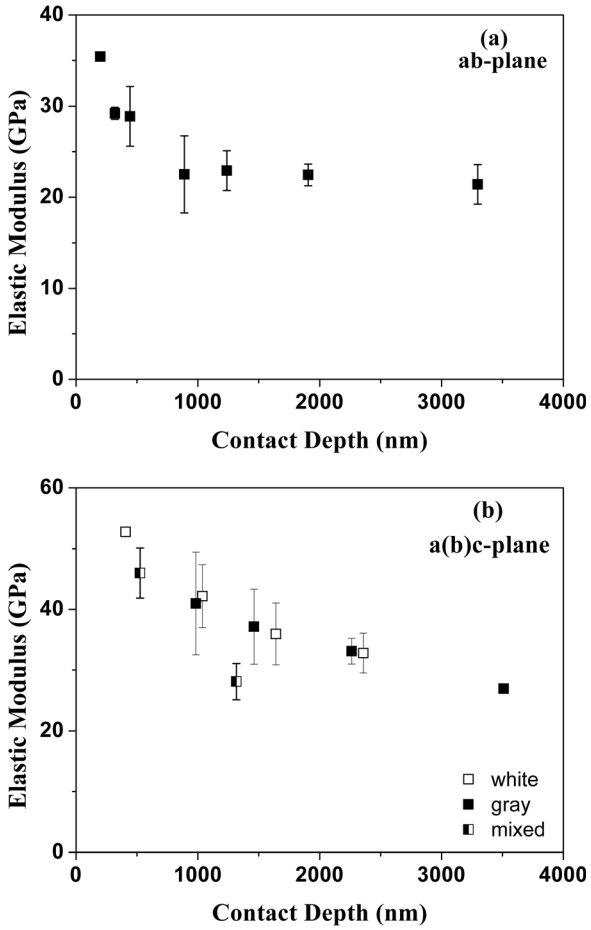

FIG. 10. Profiles of the elastic modulus as a function of contact depth for $FeSe_{0.5}Te_{0.5}$ in the (a) *ab*-plane and (b) *a(b)c*-plane. Indentations in gray, white and mixed phases are represented by the symbols ■, □, and □, respectively.

modulus was higher near the surface and decreased with increasing the contact depth. In the *ab*-plane, the elastic modulus decreased from 30 to 20 GPa, being smaller than that for the *a(b)c*-plane. For this plane, the elastic modulus decreased from 50 to 25 GPa. These values are smaller than those measured in multiphase polycrystalline $FeSe_x$ superconductor samples, where the elastic modulus is 43 ± 6 GPa.[14,15] The measured values for the bulk modulus in $FeSe_{0.5}Te_{0.5}$ is also smaller than that theoretically predicted by Chandra and Islam[16] for a similar $FeSe_{1-x}Te_x$ compound. This calculated value ranges between 70 and 73 GPa.

Several factors may originate the observed variation of hardness and/or elastic modulus with contact depth: indentation size effect,[17] a plastic deformation layer produced by polishing or errors in the area calibration function of the indenter.[12] In the indentation size effect, the hardness increases with decreasing depth, but the elastic modulus remains constant. As in our work both properties decreased upon tip penetration, we disregard this effect as having a great influence in our measurements. The area calibration function was carefully performed using a fused silica sample and the Oliver and Pharr method before the measurements, and this error does not influence our results. While the *a(b)c*-plane samples were polished for the nanoindentations tests, the *ab*-plane was not polished. Therefore, plastic deformation at the surface does not contribute to increase the hardness near the surface in the *ab*-plane. We conclude then that the observed decrease in hardness and elastic modulus with contact depth is due to the stacking of planes parallel to the *ab*-plane as observed in Fig. 1(b). Probably the bonding between the stacking planes is not strong as in a single crystal.

IV. CONCLUSIONS

Highly oriented $FeSe_{0.5}Te_{0.5}$ superconducting samples showing plate-like crystals and with a lamellar microstructure were submitted to structural and electrical characterizations, and their mechanical properties were studied by Berkovich nanoindentations. Two phases were observed with a typically eutectic microstructure, one being richer in Te and another being richer in Se. A superconducting transition temperature $T_C \sim 14.5$ K was measured using electrical resistivity measurements. No differences in hardness and elastic modulus were observed between the two phases. The bulk hardness and elastic modulus for the *ab*- and *a(b)c*-planes were 0.6–0.8 GPa and 20–25 GPa, respectively. These values are influenced by the stacking of planes parallel to the *ab*-plane.

ACKNOWLEDGMENTS

This work was partially financed by CNPq under Contact No. 474.077/2007-1 and by FAPERGS/CNPq

under Grant No. PRONEX 10/0009-2. The authors thank Professor Dr. Carlos M. Lepienski for the use of the instrumented indentation facilities.

[1]F.-C. Hsu, J.-Y. Luo, K.-W. Yeh, T.-K. Chen, T.-W. Huang, P. M. Wu, Y.-C. Lee, Y.-L. Huang, Y.-Y. Chu, D.-C. Yan, and M.-K. Wu, Proc. Natl. Acad. Sci. U.S.A. **105**, 14262 (2008).
[2]K.-W. Lee, V. Pardo, and W. E. Pickett, Phys. Rev. B **78**, 174502 (2008).
[3]J. Ge, S. Cao, S. Shen, S. Yuan, B. Kang, and J. Zhang, Solid State Commun. **150**, 1641 (2010).
[4]P. Terzieff and K. L. Komarek, Monatsh. Chem. **109**, 651 (1978).
[5]W. Schuster, H. Mimer, and K. L. Komarek, Monatsh. Chem. **110**, 1153 (1979).
[6]M. H. Fang, H. M. Pham, B. Qjan, T. J. Liu, E. K. Vehstedt, Y. Liu, L. Spinu, and Z. Q. Mao, Phys. Rev. B **78**, 224503 (2008).
[7]K. Horigane, N. Takeshita, C. Lee, H. Hiraka, and K. Yamada, J. Phys. Soc. Jpn. **78**, 63705 (2009).
[8]W. Bao, Y. Qiu, Q. Huang, M. A. Green, P. Zajdel, M. R. Fitzsimmons, M. Zhernenkov, S. Chang, M. Fang, B. Qian, E. K. Vehstedt, J. Yang, H. M. Pham, L. Spinu, and Z. Mao, Phys. Rev. Lett. **102**, 247001 (2009).
[9]S. Li, C. Cruz, Q. Huang, Y. Chen, J. W. Lynn, J. Hu, Y.-L. Huang, F. Hsu, K.-W. Yeh, M.-K. Wu, and P. Dai, Phys. Rev. B **79**, 54503 (2009).
[10]T.-L. Xia, D. Hou, S. C. Zhao, A. M. Zhang, G. F. Chen, J. L. Luo, N. L. Wang, J. H. Wei, Z.-Y. Lu, and Q. M. Zhang, Phys. Rev. B **79**, 140510 (2009).
[11]Y. Takemura, H. Suto, N. Honda, K. Kakuno, and K. Saito, J. Appl. Phys. **81**, 5177 (1997).
[12]W. C. Oliver and G. M. Pharr, J. Mater. Res. **7**, 1564 (1992).
[13]T. J. Liu, X. Ke, B. Qian, J. Hu, D. Fobes, E. K. Vehstedt, H. Pham, J. H. Yang, M. H. Fang, L. Spinu, P. Schiffer, Y. Liu, and Z. Q. Mao, Phys. Rev. B **80**, 174509 (2009).
[14]J. L. Pimentel, A. R. Jurelo, C. E. Foerster, P. R. Júnior, and R. M. Costa, Physica C **470**, S411 (2010).
[15]J. L. Pimentel, F. C. Serbena, and A. R. Jurelo, J. Supercond. Novel Magn. **24**, 1437 (2011).
[16]S. Chandra and A. K. M. A Islam, Physica C **470**, 2072 (2010).
[17]W. W. Gerberich, N. I. Tymiak, J. C. Grunlan, M. F. Horstemeyer, and M. I. Baskes, J. Appl. Mech. **69**, 433 (2002).